Title
Metamaterials based on plasmonic nanoshells and loss-compensation using fluorescent dye molecules and quantum dots

ISBN
9780819489128

Authors
Campione, Salvatore
Capolino, Filippo

Publication Date
2012-02-09

DOI
10.1117/12.909569

Metamaterials based on plasmonic nanoshells and loss-compensation using fluorescent dye molecules and quantum dots

Salvatore Campione and Filippo Capolino*
Dept. of Electrical Engineering and Computer Science, University of California, Irvine, CA 92697-2625, USA

ABSTRACT

Composite materials based on plasmonic nanoparticles allow building metamaterials with very large effective permittivity (positive or negative) or ε-near-zero; moreover, if clustered or combined with other nanoparticles, it is possible to generate also effective magnetic permeability (positive or negative), and an ad-hoc design would result in the generation of double negative materials, and therefore backward wave propagation. However, losses are usually significant and affect the metamaterial performance. In this work, we report on the possibility of adopting fluorescent dye molecules or quantum dots, optically pumped, embedded into the dielectric cores of the employed nanoshell particles, and provide loss-compensation in ordered 3D periodic arrays at optical frequencies. Each spherical nanoshell is modeled as an electric dipole. We consider nanoparticles with gold and silver shells. We then find the modes with complex wavenumber in the metamaterial, and describe the composite material in terms of homogenized effective material parameters (refractive index and permittivity). Furthermore, in case of loss-compensation, we compare the results obtained from modal analysis with the ones computed by using two different homogenization methods: (i) Maxwell Garnett homogenization theory and (ii) Nicholson-Ross-Weir retrieval method. We show the design of two ε-near-zero metamaterials with low losses by simulating gain material made of dyes or quantum dots with realistic parameters. A brief discussion about the employment of the two kinds of active gain materials adopted here is given in the end.

Keywords: loss-compensation, mode analysis, metamaterials, plasmonic nanoshells, homogenization theory.

1. INTRODUCTION AND STATEMENT OF THE PROBLEM

Periodic arrays of plasmonic nanoparticles in three dimensions (3D) are examples of metamaterials at optical frequencies. These arrays can be employed to guide backward modes, and create artificial dielectrics, narrow band absorption, artificial magnetism, quasi-dark modes. Here we focus on 3D periodic arrays, which can be represented by effective parameters, such as permittivity and refractive index, under certain circumstances of polarization and excitation. This effective medium representation allows for the design of interesting properties at specific frequency bands, such as ε-near-zero (ENZ) metamaterials, useful for cloaking applications [1] and singularity-driven nonlinear phenomena [2], guiding waves, etc. However, losses are usually found to be significantly large and affect the metamaterial performance, thus loss-mitigation mechanisms are inherently required to overcome this issue. A possible solution involves the use of active photonic materials, such as fluorescent dye molecules (DMs) and quantum dots (QDs): the gain experienced through the emission of an active medium is capable of counteracting the metamaterial absorption losses. The usage of the gain medium with metamaterials can provide a larger effective gain than when used alone, due to the strong local field enhancement inside the metamaterials [3-4].

In this paper, we provide the analysis of loss-compensated metamaterials at optical frequencies by using DMs and QDs, in order to compare their performance. In particular, we consider 3D periodic arrays of nanoshells as in Fig. 1, designing two loss-compensated ENZ composite materials (one with each kind of gain material). We compare the results obtained from (i) modal analysis (Mode-SDA) with the ones computed by using (ii) Maxwell Garnett (MG) homogenization theory and (iii) Nicholson-Ross-Weir (NRW) retrieval method.

*f.capolino@uci.edu; phone 1 949-824-2164; http://capolino.eng.uci.edu/

Photonic and Phononic Properties of Engineered Nanostructures II,
edited by Ali Adibi, Shawn-Yu Lin, Axel Scherer, Proc. of SPIE Vol. 8269,
82691E · © 2012 SPIE · CCC code: 0277-786X/12/$18 · doi: 10.1117/12.909569

Recently, optical loss compensation has been experimentally observed in [5-6] by using Coumarin C500 and Rhodamine 6G fluorescent DMs inside the dielectric shells of randomly dispersed nanoshell particles. Note that fluorescent DMs have low emitting and absorption cross sections with respect to other active materials (e.g., QDs) and high concentrations of DMs may diminish the overall compensation due to fluorescence quenching and/or other non-radiative phenomena. Homogenized effective parameters of metamaterials made of nanoshells have been simulated in [7] by artificially setting the imaginary part of the dielectric core to fixed ideal loss/gain conditions, and in [8] by using QDs emitting in the near-infrared. In [9], it has been shown that the fluorophore IR800 has enhanced properties when adjacent to metallic nanoparticles such as nanoshells and nanorods, showing the potential for contrast enhancement in fluorescence-based bioimaging. Similarly, in [10], an emission enhancement of Ruby DMs inside the dielectric core of randomly dispersed nanoshell particles has been observed with respect to the case in absence of the metallic shell. Theoretical estimations using realistic parameters of fluorescent DMs in 3D periodic arrays of nanoshells have been analyzed in [11] (and references therein). Loss-compensation has also been shown in [12] using the fishnet structure by using epoxy doped with Rhodamine 800 fluorescent DMs, where the experimental results, along with numerical simulations, directly demonstrated that the proposed sample had mitigated losses.

Here, as already shown in [11], each nanoshell is modeled as a single electric dipole, using the single dipole approximation (SDA) [13-15], and the metal permittivity for the two employed metals is described as in Appendix A. We compute the modes following the procedure described in [14,16]. Then, for transverse polarization (with respect to the mode traveling direction), we treat the metamaterial as a homogenized medium, and study loss-mitigation techniques.

The structure of the paper is as follows. The formulation to perform modal analysis in periodic arrays of nanoparticles is summarized in Sec. 2. The dispersion diagrams for the modes in case of transverse polarization in 3D periodic arrays of nanoshells are reported in Sec. 3 (gain is not considered to be present in this section). Then, in Sec. 4, we report three possible methods to retrieve the effective parameters of the analyzed composite material. We describe loss-compensation techniques in an ENZ frequency band by using DMs or QDs in Sec. 5. Conclusions are in Sec. 6. The employed metal permittivities are described as in Appendix A. The DM and QD permittivities are described in Appendix B.

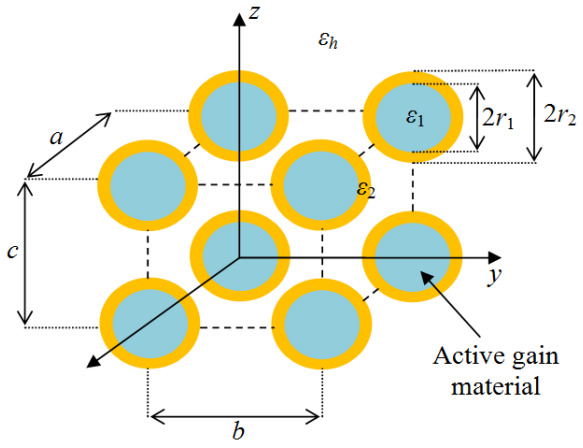

Fig. 1. 3D periodic array of nanoshells embedded in a homogeneous medium with permittivity ε_h. The core radius is r_1, with permittivity ε_1; the shell outer radius is r_2, with permittivity ε_2; a, b and c are the periodicities along x-, y- and z-direction, respectively. The two active gain materials in the cores considered here are fluorescent dye molecules and quantum dots.

2. MODE ANALYSIS IN PERIODIC ARRAYS OF NANOPARTICLES

The aim of this section is to briefly describe the formulation adopted to perform mode analysis in periodic arrays of nanoparticles. A more detailed formulation and explanation is in [14-18]. Notice that the formulation outlined here is general, and is adopted in the following sections to characterize particular array cases. The monochromatic time harmonic convention, $\exp(-i\omega t)$, is assumed and is therefore suppressed hereafter. Bold letters refer to vector quantities, a bar under a bold letter refers to dyadic quantities and a caret on top of a bold letter refers to unit vectors.

According to SDA, each plasmonic nanoparticle at optical frequencies acts as a single electric dipole and can be described by its induced electric dipole moment

$$\mathbf{p} = \boldsymbol{\alpha}_{\mathrm{ee}} \mathbf{E}^{\mathrm{loc}}, \tag{1}$$

where $\boldsymbol{\alpha}_{\mathrm{ee}}$ is the electric polarizability tensor of the nanoparticle, and $\mathbf{E}^{\mathrm{loc}}$ is the local field acting on it [14-15]. For isotropic nanoparticles (e.g., spherical), the polarizability tensor $\boldsymbol{\alpha}_{\mathrm{ee}}$ degenerates into a diagonal matrix with entrance α_{ee}. For nanoshells, and according to Mie theory [13,19], it follows that

$$\alpha_{\mathrm{ee}} = \frac{6\pi i \varepsilon_h \varepsilon_0}{k^3} \frac{\psi_1(kr_2)A - m_2\psi_1'(kr_2)B}{\xi_1(kr_2)A - m_2\xi_1'(kr_2)B}, \quad A = \psi_1'(m_2 kr_2) - C\chi_1'(m_2 kr_2) \tag{2}$$

and

$$B = \psi_1(m_2 kr_2) - C\chi_1(m_2 kr_2), \quad C = \frac{m_2\psi_1(m_2 kr_1)\psi_1'(m_1 kr_1) - m_1\psi_1'(m_2 kr_1)\psi_1(m_1 kr_1)}{m_2\chi_1(m_2 kr_1)\psi_1'(m_1 kr_1) - m_1\chi_1'(m_2 kr_1)\psi_1(m_1 kr_1)}, \tag{3}$$

with $\psi_1(\rho) = \rho j_1(\rho) = \sin\rho/\rho - \cos\rho$, $\xi_1(\rho) = \rho h_1^{(1)}(\rho) = (-i/\rho - 1)e^{i\rho}$ and $\chi_1(\rho) = -\rho y_1(\rho) = \cos\rho/\rho + \sin\rho$ the Riccati-Bessel functions [20] (a prime denotes a derivative with respect to the argument), ε_h is the relative permittivity of the host medium, $k = \omega\sqrt{\varepsilon_h}/c_0 = k_0\sqrt{\varepsilon_h}$ is the host wavenumber, where k_0 denotes the free space wavenumber, c_0 the speed of light, ε_0 is the free space absolute permittivity and $m_1 = \sqrt{\varepsilon_1/\varepsilon_h}$, $m_2 = \sqrt{\varepsilon_2/\varepsilon_h}$ are the core and shell relative refractive indexes, with ε_1 the relative permittivity of the core (of internal radius r_1), and ε_2 the relative permittivity of the shell (of external radius r_2). The relative permittivity of the two metals employed here is modeled as outlined in Appendix A.

Consider now a periodic array of nanoparticles, immersed in a homogeneous background, with relative permittivity ε_h, for which each nanoparticle is placed at positions $\mathbf{r}_n = \mathbf{r}_0 + \mathbf{d}_n$, where $n \equiv n_1, n_2, n_3 = 0, \pm 1, \pm 2, ...,$ is a triple index, and $\mathbf{d}_n = n_1 a\hat{\mathbf{x}} + n_2 b\hat{\mathbf{y}} + n_3 c\hat{\mathbf{z}}$ in 3D periodic arrays, $\mathbf{r}_0 = x_0\hat{\mathbf{x}} + y_0\hat{\mathbf{y}} + z_0\hat{\mathbf{z}}$, and a, b and c are the 3D periodicities along x-, y- and z-direction, respectively. Suppose that the array is either excited or a mode (a periodic field) is present, with wavevector $\mathbf{k}_{\mathrm{B}} = k_x\hat{\mathbf{x}} + k_y\hat{\mathbf{y}} + k_z\hat{\mathbf{z}}$. Consequently, each nanoparticle will have a dipole moment equal to $\mathbf{p}_n = \mathbf{p}_0 e^{i\mathbf{k}_{\mathrm{B}}\cdot\mathbf{d}_n}$. Then, the local field acting in absence of excitation on a nanosphere at position $\mathbf{r}_0 = \mathbf{0}$ is given by

$$\mathbf{E}^{\mathrm{loc}}(\mathbf{r}_0, \mathbf{k}_{\mathrm{B}}) = \breve{\underline{\mathbf{G}}}^{\infty}(\mathbf{r}_0, \mathbf{r}_0, \mathbf{k}_{\mathrm{B}}) \cdot \mathbf{p}_0, \tag{4}$$

which represents the electric field produced by all the nanoparticles but the one at position $\mathbf{r}_0$, and $\breve{\underline{\mathbf{G}}}^{\infty}(\mathbf{r}_0, \mathbf{r}_0, \mathbf{k}_{\mathrm{B}})$ represents the regularized periodic dyadic Green's function (GF). The computation of this GF for 1D periodic arrays can be found in [17], in [21] for 2D periodic arrays, and in [16] for 3D periodic arrays. We have found very convenient to use the Ewald method to represent the periodic GF in periodic structures. The Ewald method allows for a very rapid convergence of the GF series representation, and analytic continuation into the complex $\mathbf{k}_{\mathrm{B}}$ wavenumber domain, which is required when searching for complex wavenumbers.

Substituting then the expression for the local field given in (4) into (1), it follows that

$$\mathbf{p}_0 = \alpha_{\mathrm{ee}} \breve{\underline{\mathbf{G}}}^{\infty}(\mathbf{r}_0, \mathbf{r}_0, \mathbf{k}_{\mathrm{B}}) \cdot \mathbf{p}_0, \tag{5}$$

which leads to the linear system

$$\underline{\mathbf{A}}(\mathbf{k}_{\mathrm{B}}) \cdot \mathbf{p}_0 = \mathbf{0}, \qquad \underline{\mathbf{A}}(\mathbf{k}_{\mathrm{B}}) = \underline{\mathbf{I}} - \alpha_{\mathrm{ee}} \breve{\underline{\mathbf{G}}}^{\infty}(\mathbf{r}_0, \mathbf{r}_0, \mathbf{k}_{\mathrm{B}}). \tag{6}$$

The properties of $\underline{\mathbf{A}}(\mathbf{k}_B)$ can be found in [16-18]. The mode dispersion analysis in the periodic array is then obtained by computing the complex $\mathbf{k}_B$ of the homogeneous linear system in (6), or, in other words, by solving

$$\det\left[\underline{\mathbf{A}}(\mathbf{k}_B)\right] = 0 \tag{7}$$

for complex $\mathbf{k}_B$.

3. MODE DISPERSION DIAGRAMS FOR 3D PERIODIC ARRAYS OF NANOSHELLS

We study here the two structures reported in Table 1, where Structure I has nanoparticles with gold shells and cores with DMs, and Structure II silver shells with QD cores. The parameters have been designed keeping in mind the objective of an ENZ composite material with low losses around 430 THz (see details in Sec. 5), which corresponds to a free space wavelength of 698 nm. The choice of gold in the first case and silver in the second one is an authors' choice; other designs may provide with results similar to the shown ones. Note also the need of designing two different structures because of the following reason: large concentrations of DMs are needed to provide enough gain, thus Structure I needs to have nanoshells' cores to contain them, and each nanoparticles has a diameter of 70 nm. Conversely, small QDs of nanometer size already provide sufficient gain, therefore much smaller dimensions for Structure II need to be designed, and each nanoparticle has a diameter of just 10 nm.

Table 1. Parameters of the two analyzed 3D periodic arrays of nanoshells to achieve ENZ behavior around 430 THz.

Structure	Metal shell	Gain material core	Core radius r_1 [nm]	Outer shell radius r_2 [nm]	Core permittivity ε_1	Shell permittivity ε_2	ε_h	a,b,c [nm]
I	Gold	Dye molecules	30	35	ε_g (Sec. 5.1)	ε_m (Appendix A)	2.25	100
II	Silver	Quantum dots	4	5	ε_{QD} (Sec. 5.2)	ε_m (Appendix A)	2.25	15

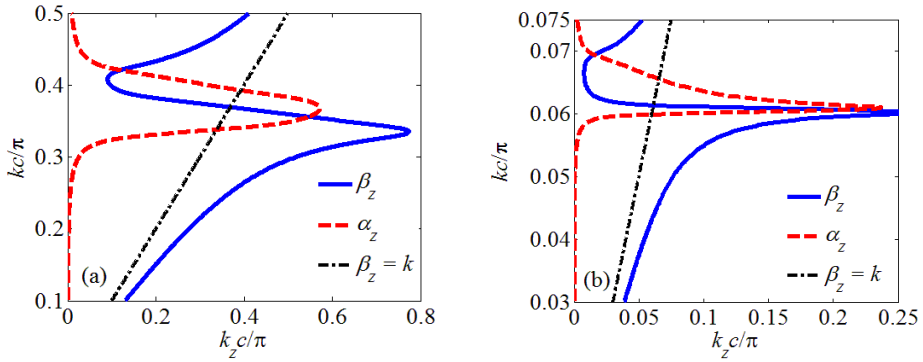

Fig. 2. Dispersion diagram, obtained by solving (7), for both the real and the imaginary part of the wavenumber $k_z = \beta_z + i\alpha_z$ versus the host wavenumber k for transverse polarization, using the nanoshell Mie polarizability in (2), for (a) Structure I and (b) Structure II, in absence of gain.

The dispersion diagrams for the two proposed structures in absence of gain (i.e., transparent condition, that is $\varepsilon_1 = 2.25$ for Structure I and $\varepsilon_1 = 5.9$ for Structure II) are shown in Fig. 2 for both the real (solid blue curve) and the imaginary (dashed red curve) parts of the wavenumber $k_z = \beta_z + i\alpha_z$ of the "dominant" mode (i.e., the one that contributes most to the field in the array, see [16] for a detailed study in a 3D periodic array of plasmonic nanospheres) with respect to the host wavenumber k in the case of transverse polarization. We assume $k_x = k_y = 0$, i.e, propagation along the z

direction only. In each graph, only the mode with $\alpha_z \geq 0$, i.e., the one with power flow toward the positive *z*-direction, is shown (for reference we report also the light line $\beta_z = k$ as the dashed-dotted black curve). This mode follows a typical dispersion curve which is almost straight at low frequencies corresponding to an effective medium slightly denser than the host medium with small attenuation; then, increasing the frequency, the dispersion curve bends exhibiting large phase constant. Further increasing frequency, it experiences a bandgap with a strong attenuation; finally, at higher frequencies it reenters a propagation band with small attenuation. Note however that other modes with attenuation constant larger than the one shown here are present, but not reported here since they dramatically decay as $\alpha_z >> k$.

4. EFFECTIVE PARAMETERS OF HOMOGENIZED MEDIA

The aim of this section is to summarize the three methods that are used in Sec. 5 to retrieve the effective parameters of homogenized media: modal analysis (Mode-SDA), Maxwell Garnett (MG) and Nicholson-Ross-Weir (NRW) retrieval method. Note that both Mode-SDA and MG use the nanoshells' Mie polarizability in (2).

4.1 Mode analysis (Mode-SDA)

Assume that it is possible to compute the modes that could be excited in a specific composite slab (as proposed in Sec. 2), and that furthermore this could be treated as a homogeneous material. The effective refractive index can be then computed as

$$n_{\text{eff}} = \frac{k_z}{k_0} \tag{8}$$

where k_z is the complex wavenumber of the "dominant" mode (as the one shown in Fig. 2 for the 3D periodic array of nanoshells in Sec. 3) computed from modal analysis (i.e., by solving (7)), and k_0 is the free space wavenumber. Moreover, at plasmonic frequencies, for this kind of composite materials, magnetic effects are negligible, thus one can compute the effective relative permittivity as $\varepsilon_{\text{eff}} \approx n_{\text{eff}}^2$ with good approximation.

4.2 Maxwell Garnett (MG)

In general, Maxwell Garnett theory [22-24] can be applied to retrieve the relative effective permittivity of a composite medium as

$$\varepsilon_{\text{eff}} = \varepsilon_h + \frac{\varepsilon_h}{N_D^{-1}\varepsilon_0\varepsilon_h\left[\alpha_{\text{ee}}^{-1} + i\frac{k^3}{6\pi\varepsilon_0\varepsilon_h}\right] - \frac{1}{3}} \tag{9}$$

where $N_D = f / V_N$, with f the volume filling fraction of the mixture, V_N is the volume of each inclusion (the nanoparticle). Note that in (9) the dipolar radiative loss term $-ik^3/(6\pi)$ has been subtracted, to account for the cancellation of scattering losses in a periodic metamaterial [25], whereas the procedure leading to the electric polarizability in Sec. 2 includes all radiation losses. More details about Maxwell Garnett homogenization theory can be found in [26-29].

4.3 Nicolson-Ross-Weir (NRW)

Transmission and reflection coefficients for a stack of layers are here used to retrieve the effective refractive index of the composite material by using the Nicholson-Ross-Weir (NRW) method [30-35]. Treating the composite slab as a uniform continuous medium with same thickness *t*, according to NRW, the complex effective refractive index can be retrieved by

$$n_{\text{eff}} = \pm\frac{\cos^{-1}\left(\frac{1-R^2+T^2}{2T}\right)}{k_0 t} + \frac{2\pi q}{k_0 t}, \tag{10}$$

where *R* and *T* are the complex reflection and transmission coefficients, q is an integer to be determined, and $t = Nc$ is the equivalent thickness of the metamaterial sample, with N denoting the number of layers and c the separation between two contiguous layers. We address the reader to [33-34] for guidelines on how to choose *q* and +/- in (10). As in

Sec. 4.1, we recall that at plasmonic frequencies the magnetic effects are negligible, thus one can compute the effective relative permittivity as $\varepsilon_{\text{eff}} \approx n_{\text{eff}}^2$ with good approximation.

We analyze propagation for Structure I in Table 1 made of 4 layers of nanoshells stacked along the *z*-direction (in presence of gain in the nanoshell cores as described in Sec. 5.1), by using (i) HFSS and (ii) the SDA with the Mie polarizability in (2). The stack is illuminated by a normally incident plane wave traveling toward +*z*, and the magnitude of transmission *T* and reflection *R* of the stack are shown in Fig. 3, together with the absorption $A = 1 - |T|^2 - |R|^2$. Results in Fig. 3 show good agreement between the HFSS full-wave simulation and the SDA theoretical results. In the evaluation of the SDA results we have used the Ewald representation of the dyadic GF for 2D periodic arrays reported in [21].

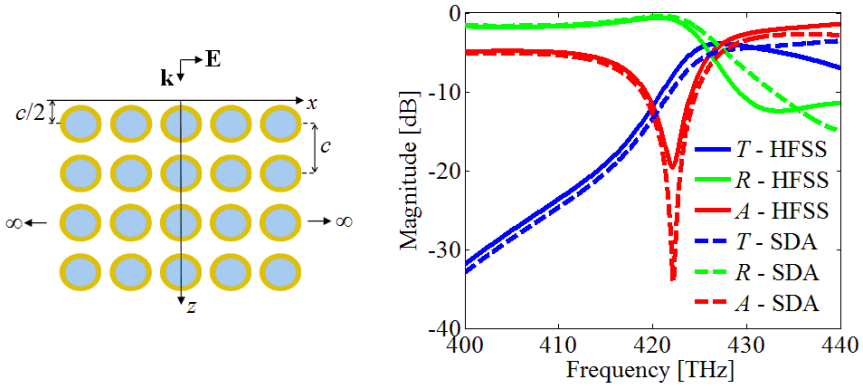

Fig. 3. Magnitude of transmission *T*, reflection *R* and absorption *A* coefficients for a stack of 4 layers of Structure I in Table 1 (only a transverse cut in the *xz* plane of a 3D array is shown), in presence of gain as in Sec. 5.1. Results obtained by using the SDA and HFSS are in agreement.

5. EFFECTIVE ENZ FREQUENCY BAND IN 3D PERIODIC ARRAYS OF NANOSHELLS IN PRESENCE OF LOSS-COMPENSATION

The aim of this section is to alleviate propagation losses in a frequency region in which the real part of epsilon is close to zero (either negative or positive), by using either fluorescent DMs or QDs. Results are compared by using the three analysis methods outlined in Sec. 4. In this section, the results retrieved using the NRW method are based on reflection and transmission coefficients computed by HFSS.

5.1 Fluorescent dye molecules (DMs)

In this subsection, we assume that Rhodamine 800 dye molecules are dispersed into the dielectric core of the nanoshells. We assume here that the collection of the fluorescent dyes within the core can be approximated as an effective homogeneous material (modeled with relative permittivity ε_g, see also Appendix B) with gain that electrodynamically interacts with the metal nanoparticle (i.e., quenching effect and other non-radiative phenomena *within the core*, whose effects increase for increasing molecular concentration, that usually lead to a reduction of the gain in the system, are not taken into account).

Gain materials are described by using the same four energy level system formulation as in [11], that at stationary regime provides (plotted in Appendix B)

$$\varepsilon_g = \varepsilon_r + \frac{\sigma_e}{\omega^2 + i\Delta\omega_e\omega - \omega_e^2} \frac{(\tau_{21} - \tau_{10})\Gamma_{\text{pump}}}{1 + (\tau_{32} + \tau_{21} + \tau_{10})\Gamma_{\text{pump}}} \frac{\bar{N}_0}{\varepsilon_0}, \tag{11}$$

where $\varepsilon_r = 2.25$ is the relative permittivity of the dielectric hosting the DMs, $\omega_e = 2\pi f_e$, with center emission frequency $f_e = 422$ THz (711 nm), wavelength linewidth is $\Delta\lambda_e = 26.7$ nm, and consequently $\Delta\omega_e = 2\pi\Delta f_e$, with frequency linewidth $\Delta f_e = c_0 \Delta\lambda_e / \lambda_e^2 = 15.9$ THz. The pumping wavelength (between level 0 and level 3) is 680 nm

(441 THz), and the decay rate from level 2 to level 1 is $1/\tau_{21}$, with $\tau_{21} = 500$ ps, $\tau_{32} = \tau_{10} = 100$ fs. The coupling constant is $\sigma_e = 1.71\times10^{-7}$ C^2/kg. We set the density of dye molecules as $\bar{N}_0 = 6\times10^{18}$ cm^{-3} corresponding to about a concentration of 10 mM (which corresponds to a high concentration value) and the pumping rate to be $\Gamma_{\text{pump}} = 6.5\times10^{9}$ s^{-1}.

We study here Structure I in Table 1 in presence of gain. We are interested in alleviating propagation losses in an ENZ frequency region. The effective refractive index and relative permittivity are shown in Figs. 4 and 5.

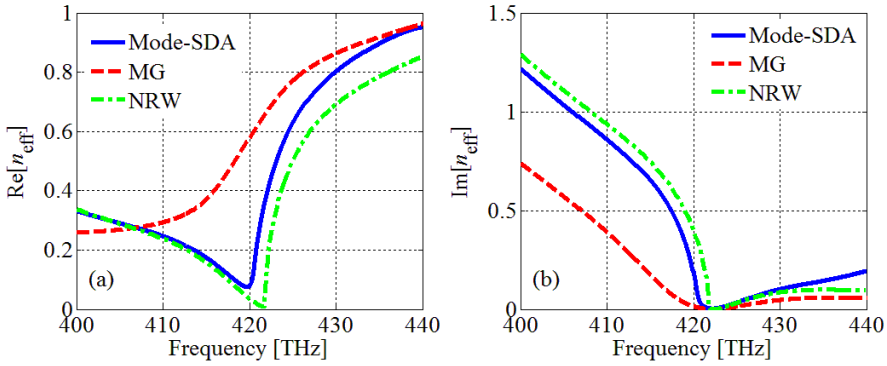

Fig. 4. (a) Real part and (b) imaginary part of the effective refractive index around the ENZ frequency band for Structure I in presence of gain computed in three different ways: by mode analysis (Mode-SDA); by Maxwell Garnett, by using the polarizability in (2) (MG); and by Nicholson-Ross-Weir (NRW) method based on HFSS results.

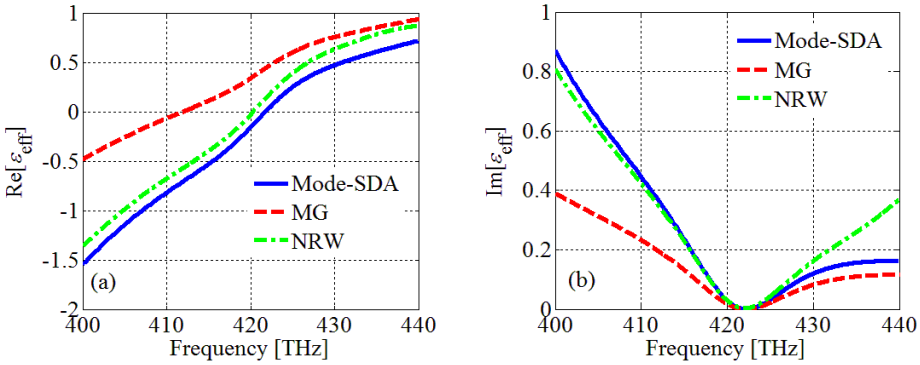

Fig. 5. (a) Real part and (b) imaginary part of the effective relative permittivity around the ENZ frequency band for Structure I in presence of gain computed in three different ways: by mode analysis (Mode-SDA); by Maxwell Garnett, by using the polarizability in (2) (MG); and by Nicholson-Ross-Weir (NRW) method based on HFSS results.

Notice how the Mode-SDA and NRW results in Figs. 4 and 5 are in good agreement with each other. The result computed using MG provides less accurate values because field retardation effects between nanoparticle interactions are not included. Notice that with NRW the zero crossing of the real part of the effective relative permittivity happens at a frequency slightly lower than the one predicted by the Mode-SDA: however, this can be adjusted by performing a fine-tuning of the nanoshells volume filling fraction, as proposed in [8]. Note also how the $\text{Im}[\varepsilon_{\text{eff}}]$ around 422 THz in the loss-compensated case is very small in value (close to zero). Indeed, we have performed an HFSS simulation for the same array in absence of losses (not reported), and by using the NRW result, we have observed a reduction of the extinction coefficient $\text{Im}[n_{\text{eff}}]$ from 0.33 to 3.5×10^{-4} at $f \approx 422$ THz, in the ENZ frequency band. The figure of merit $\text{Re}[n_{\text{eff}}]/\text{Im}[n_{\text{eff}}]$ in presence and in absence of loss-compensation is shown in Fig. 6, obtained from NRW result, and it shows clearly higher values in the case of loss-compensation.

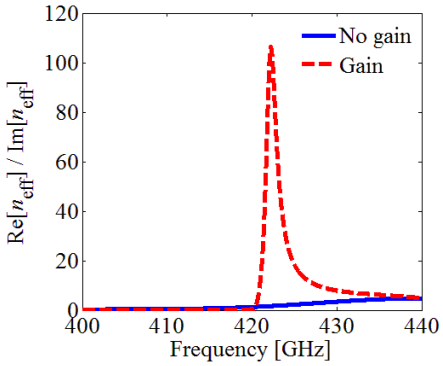

Fig. 6. Figure of merit $\mathrm{Re}\left[n_{\mathrm{eff}}\right] / \mathrm{Im}\left[n_{\mathrm{eff}}\right]$ for Structure I, obtained from NRW result, with and without gain.

5.2 Quantum dots

In this subsection, we assume that an InP/ZnS QD with the physical dimensions as in [36] constitutes the core of each nanoshell. The QD dielectric function in presence of gain, assumed to be homogeneous, is calculated using the formalism in [36-37] as

$$\varepsilon_{\mathrm{QD}} = \varepsilon_b + \frac{S}{\omega^2 - \omega_e^2 + i2\omega\gamma}, \tag{12}$$

with the realistic data taken from [36]: background dielectric constant $\varepsilon_b = 5.9$, emission at $f_e \approx 444$ THz, broadening parameter $\gamma \approx 7.59\times10^{12}\,\mathrm{s}^{-1}$, and $S = 4\pi s f_e$, with transition strength $s \approx 1.38\times10^{13}$ rad/s (see also Appendix B).

We study here Structure II in Table 1 in presence of gain. We then focus again on an ENZ frequency band and the effective refractive index and relative permittivity are shown in Figs. 7 and 8.

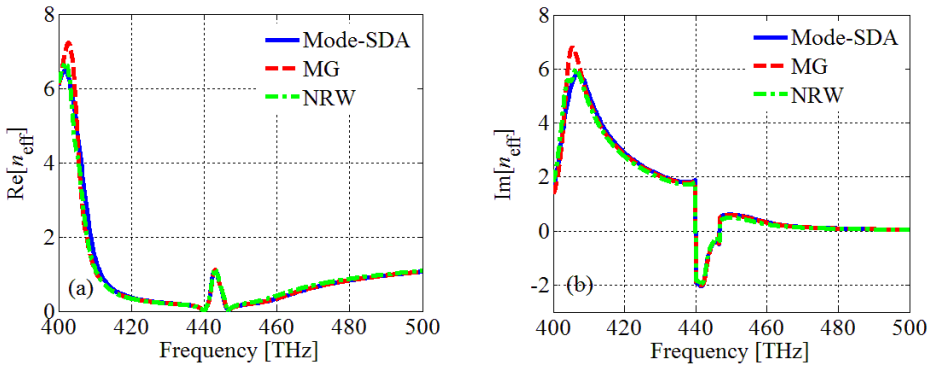

Fig. 7. (a) Real part and (b) imaginary part of the effective refractive index around the ENZ frequency band for Structure II in presence of gain computed in three different ways: by mode analysis (Mode-SDA); by Maxwell Garnett, by using the polarizability in (2) (MG); and by Nicholson-Ross-Weir (NRW) method based on HFSS results.

The three methods provide with results in good agreement with each other. Note the resonant behavior of the real part introduced by the presence of the QD, which also is the reason of the negative peak in the imaginary part. Two interesting regions can be analyzed, one with $\mathrm{Im}\left[\varepsilon_{\mathrm{eff}}\right] < 0$ (i.e., gain) and one with $\mathrm{Im}\left[\varepsilon_{\mathrm{eff}}\right] > 0$ (i.e., loss-compensation). A negative $\mathrm{Im}\left[\varepsilon_{\mathrm{eff}}\right]$ is observed between about 440 – 446 THz, which means that amplification is present in the system. Instabilities and overall gain should be further studied in the future. However, this result shows over-compensation capabilities, thus opening up possibility to efficient loss-compensated designs. A positive $\mathrm{Im}\left[\varepsilon_{\mathrm{eff}}\right]$ is observed in the frequency range 436.5 – 440 THz, where the real

part is negative around the value –3.5, and in the range 446 – 460 THz, where the real part is close to zero (between –0.3 and 0).

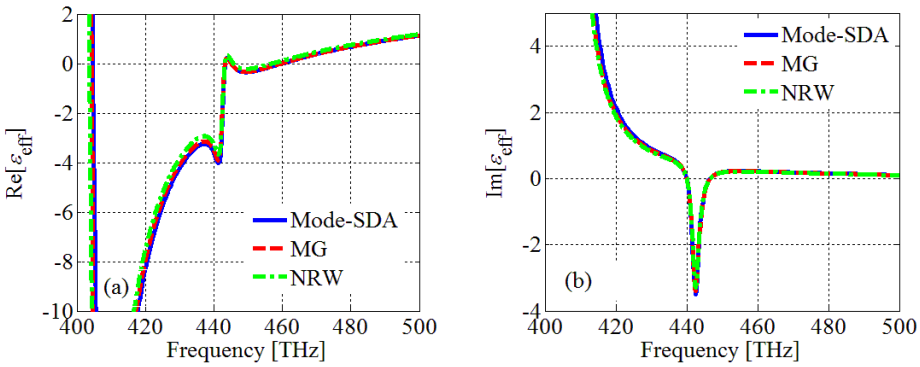

Fig. 8. (a) Real part and (b) imaginary part of the effective relative permittivity around the ENZ frequency band for Structure II in presence of gain computed in three different ways: by mode analysis (Mode-SDA); by Maxwell Garnett, by using the polarizability in (2) (MG); and by Nicholson-Ross-Weir (NRW) method based on HFSS results.

6. CONCLUSION

We have studied the modal dispersion diagrams in 3D periodic arrays of nanoshells for transverse polarization with respect to the direction of propagation. Under this polarization, we have embedded an active gain material made of either fluorescent dye molecules or quantum dots into the nanoshell cores. By using realistic parameters to model their permittivity versus frequency, we have designed two ENZ metamaterials with loss-compensation mechanisms around 430 THz. In the case of dye molecules, we have been able to reduce the extinction coefficient $\mathrm{Im}[n_{\mathrm{eff}}]$ from 0.33 to 3.5×10^{-4}, according to the NRW result based on HFSS full-wave simulation. In the case of quantum dots, we have observed loss-compensation and even amplification (i.e., over-compensation capabilities) thus opening up possibility to efficient loss-compensated designs or possible lasing systems using composite materials. The results shown in this paper demonstrate the possibility to obtain ENZ metamaterials with virtually zero losses in specific frequency bands.

APPENDIX A: HOW TO MODEL THE METAL PERMITTIVITY AT OPTICAL FREQUENCIES

The relative permittivity of the metal can be analytically modeled using several equations to match the experimental results provided by Johnson and Christy in [38].

One of these equations is the Drude model

$$\varepsilon_m = \varepsilon_\infty - \frac{\omega_p^2}{\omega(\omega + i\gamma)} \tag{13}$$

where ε_∞ is a high-frequency fitting parameter, ω_p is the plasma frequency of the metal (expressed in rad/s) and γ is the damping factor (expressed in s^{-1}). In general, the Drude model provides a reasonably accurate description of the dielectric properties of the metal across the infrared and optical frequency ranges (focus of this paper). For some frequency bands, this model underestimates the metal absorption, and the effect of interband transitions should be taken into account in the metal permittivity response [39].

The adopted Drude parameters to model gold and silver as in (13) are reported in Table 2.

Table 2. Drude model parameters for gold and silver.

Metal	ε_∞	ω_p [rad/s]	γ [1/s]
Gold	9.5	1.36×10^{16}	1.05×10^{14}
Silver	5	1.37×10^{16}	27.3×10^{12}

The real and imaginary parts of the relative permittivity computed with (13) for gold and silver using the parameters in Table 2 are compared with the experimental results provided by Johnson and Christy in [38] in Figs. 9 and 10 in a frequency band of interest to this paper. Note that for gold the real part is well modeled in the entire frequency range; as previously mentioned, instead, the model underestimates the imaginary part for increasing frequency. However, the ENZ frequency band under analysis in Sec. 5.1 is in the range 400 – 440 THz, so we can assume that the gold behavior is well modeled by the Drude model. Regarding silver, instead, the Drude model roughly approximates the experimental results across the frequency range 400 – 500 THz used in Sec. 5.2. Therefore, in this paper we use (13) to model the gold permittivity, and an interpolation of the experimental data in [38] to model the silver permittivity.

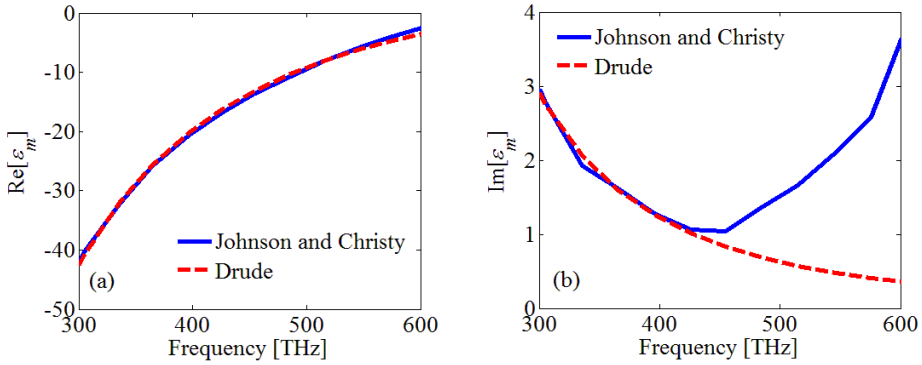

Fig. 9. (a) Real and (b) imaginary part of the permittivity of gold retrieved using (13) with the parameters in Table 2, compared to the experimental results in [38].

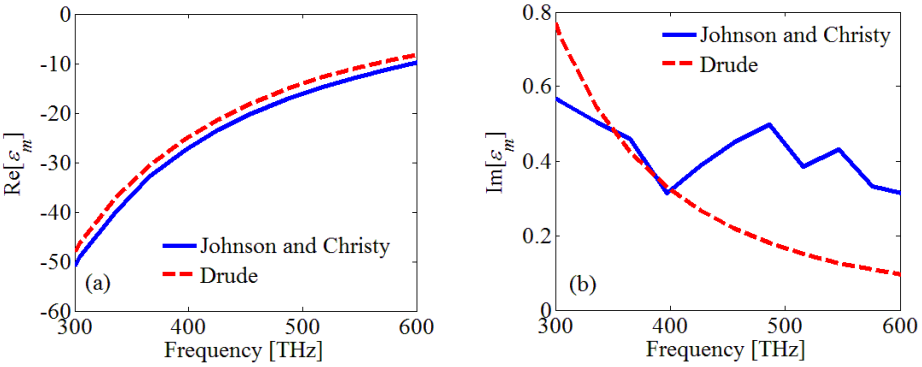

Fig. 10. As in Fig. 9, for silver.

APPENDIX B: BRIEF DISCUSSION ON FLUORESCENT DYE MOLECULES AND QUANTUM DOTS

We report in Fig. 11 the real and the imaginary parts of the relative permittivity of DMs in (11) and QDs in (12). Note that QDs have a more pronounced and narrower resonance than DMs: this means that QDs strongly modify the metamaterial behavior with respect to the case without gain. Also, DMs provide less gain (as dictated by the smaller $|\mathrm{Im}[\varepsilon]|$).

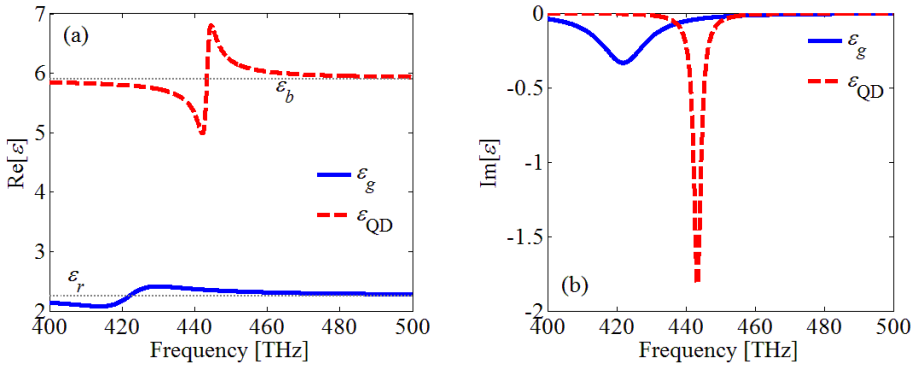

Fig. 11. (a) Real and (b) imaginary part of the permittivity describing the two active gain materials employed in this paper.

ACKNOWLEDGEMENT

The authors acknowledge partial support from the National Science Foundation (NSF)-CMMI award 1101074. The authors also thank Ansys for providing HFSS.

REFERENCES

[1] M. G. Silveirinha, A. Alu, B. Edwards, and N. Engheta, "Overview of theory and applications of epsilon-near-zero materials," *URSI General Assembly,* Chicago, IL (2008).

[2] M. A. Vincenti, D. d. Ceglia, A. Ciattoni, and M. Scalora, "Singularity-driven second and third harmonic generation at ε-near-zero crossing points," *Physical Review A,* 84, 063826 (2011).

[3] D. J. Bergman, and M. I. Stockman, "Surface plasmon amplification by stimulated emission of radiation: Quantum generation of coherent surface plasmons in nanosystems," *Physical Review Letters,* 90(2), 027402 (2003).

[4] M. I. Stockman, "Spasers explained," *Nature Photonics,* 2(6), 327-329 (2008).

[5] G. Strangi, A. De Luca, S. Ravaine, M. Ferrie, and R. Bartolino, "Gain induced optical transparency in metamaterials," *Applied Physics Letters,* 98(25), 251912 (2011).

[6] A. De Luca, M. P. Grzelczak, I. Pastoriza-Santos, L. M. Liz-Marzán, M. La Deda, M. Striccoli, and G. Strangi, "Dispersed and encapsulated gain medium in plasmonic nanoparticles: a multipronged approach to mitigate optical losses," *ACS Nano,* 5(7), 5823-5829 (2011).

[7] J. A. Gordon, and R. W. Ziolkowski, "CNP optical metamaterials," *Optics Express,* 16(9), 6692-6716 (2008).

[8] A. Ciattoni, R. Marinelli, C. Rizza, and E. Palange, "|ε|-near-zero materials in the near-infrared," *arxiv:1107.5540* (2011).

[9] R. Bardhan, N. K. Grady, J. R. Cole, A. Joshi, and N. J. Halas, "Fluorescence enhancement by Au nanostructures: nanoshells and nanorods," *ACS Nano,* 3(3), 744-752 (2009).

[10] J. Zhang, I. Gryczynski, Z. Gryczynski, and J. R. Lakowicz, "Dye-labeled silver nanoshell−bright particle," *The Journal of Physical Chemistry B,* 110(18), 8986-8991 (2006).

[11] S. Campione, M. Albani, and F. Capolino, "Complex modes and near-zero permittivity in 3D arrays of plasmonic nanoshells: loss compensation using gain [Invited]," *Opt. Mater. Express,* 1(6), 1077-1089 (2011).

[12] S. Xiao, V. P. Drachev, A. V. Kildishev, X. Ni, U. K. Chettiar, H.-K. Yuan, and V. M. Shalaev, "Loss-free and active optical negative-index metamaterials," *Nature,* 466(7307), 735-738 (2010).

[13] C. F. Bohren, and D. R. Huffman, [Absorption and Scattering of Light by Small Particles] Wiley, New York (1983).

[14] S. Steshenko, and F. Capolino, "Single dipole approximation for modeling collections of nanoscatterers," in [Theory and Phenomena of Metamaterials], F. Capolino, ed., CRC Press, Boca Raton, FL, Chapter 8 (2009).

[15] S. Campione, and F. Capolino, "Linear and Planar Periodic Arrays of Metallic Nanospheres: Fabrication, Optical Properties and Applications," in [Selected Topics in Metamaterials and Photonic Crystals], A.

Andreone, A. Cusano, A. Cutolo and V. Galdi, eds., World Scientific Publishing, Hackensack, NJ, Chapter 5 (2011).
[16] S. Campione, S. Steshenko, M. Albani, and F. Capolino, "Complex modes and effective refractive index in 3D periodic arrays of plasmonic nanospheres," *Optics Express,* 19(27), 26027-26043 (2011).
[17] S. Campione, S. Steshenko, and F. Capolino, "Bound and leaky modes in chains of plasmonic nanospheres," *Optics Express,* 19(19), 18345-18363 (2011).
[18] A. L. Fructos, S. Campione, F. Capolino, and F. Mesa, "Characterization of complex plasmonic modes in two-dimensional periodic arrays of plasmonic nanospheres," *Journal of the Optical Society of America B,* 28(6), 1446-1458 (2011).
[19] S. Campione, S. Pan, S. A. Hosseini, C. Guclu, and F. Capolino, "Electromagnetic metamaterials as artificial composite structures," in [Handbook of Nanoscience, Engineering, and Technology], W. A. Goddard III, D. Brenner, S. E. Lyshevski, and G. J. Iafrate, eds., CRC Press, Boca Raton, FL, Chapter 21 (in print, 2012).
[20] M. Abramowitz, and I. A. Stegun, [Handbook of Mathematical Functions with Formulas, Graphs, and Mathematical Tables] Dover Publications, New York (1965).
[21] S. Steshenko, F. Capolino, P. Alitalo, and S. Tretyakov, "Effective model and investigation of the near-field enhancement and subwavelength imaging properties of multilayer arrays of plasmonic nanospheres," *Physical Review E,* 84(1), 016607 (2011).
[22] A. Sihvola, [Electromagnetic Mixing Formulas and Applications] IEEE Publishing, London (1999).
[23] A. Sihvola, "Mixing rules," in [Theory and Phenomena of Metamaterials], F. Capolino, ed., CRC Press, Boca Raton, FL, Chapter 9 (2009).
[24] V. Yannopapas, and A. Moroz, "Negative refractive index metamaterials from inherently non-magnetic materials for deep infrared to terahertz frequency ranges," *Journal of Physics: Condensed Matter,* 17(25), 3717 (2005).
[25] S. Tretyakov, [Analytical Modeling in Applied Electromagnetics] Artech House, Boston (2003).
[26] W. T. Doyle, "Optical properties of a suspension of metal spheres," *Physical Review B,* 39(14), 9852 (1989).
[27] R. Ruppin, "Evaluation of extended Maxwell-Garnett theories," *Optics Communications,* 182(4-6), 273-279 (2000).
[28] L. Lewin, "The electrical constants of a material loaded with spherical particles," *Journal of the Institution of Electrical Engineers. III. Radio and Communication Engineering,* 94(27), 65-6868 (1947).
[29] A. Lakhtakia, and W. S. Weiglhofer, "Maxwell-Garnett estimates of the effective properties of a general-class of discrete random composites," *Acta Crystallographica Section A,* 49, 266-269 (1993).
[30] A. M. Nicolson, and G. F. Ross, "Measurement of the intrinsic properties of materials by time-domain techniques," *IEEE Transactions on Instrumentation and Measurement,* 19(4), 377-382 (1970).
[31] W. B. Weir, "Automatic measurement of complex dielectric constant and permeability at microwave frequencies," *Proceedings of the IEEE,* 62(1), 33-36 (1974).
[32] A. H. Boughriet, C. Legrand, and A. Chapoton, "Noniterative stable transmission/reflection method for low-loss material complex permittivity determination," *IEEE Transactions on Microwave Theory and Techniques,* 45(1), 52-57 (1997).
[33] D. R. Smith, S. Schultz, P. Markoscaron, and C. M. Soukoulis, "Determination of effective permittivity and permeability of metamaterials from reflection and transmission coefficients," *Physical Review B,* 65(19), 195104 (2002).
[34] C. R. Simovski, "On the extraction of local material parameters of metamaterials from experimental or simulated data," in [Theory and Phenomena of Metamaterials], F. Capolino, ed., CRC Press, Boca Raton, FL, Chapter 11 (2009).
[35] S. A. Ramakrishna, and T. M. Grzegorczyk, [Physics and Applications of Negative Refractive Index Materials] CRC Press and SPIE Press, Boca Raton, FL (2009).
[36] P. Holmstrom, L. Thylen, and A. Bratkovsky, "Composite metal/quantum-dot nanoparticle-array waveguides with compensated loss," *Applied Physics Letters,* 97(7), 073110 (2010).
[37] P. Holmstrom, L. Thylen, and A. Bratkovsky, "Dielectric function of quantum dots in the strong confinement regime," *Journal of Applied Physics,* 107(6), 064307-7 (2010).
[38] P. B. Johnson, and R. W. Christy, "Optical constants of the noble metals," *Physical Review B,* 6(12), 4370 (1972).
[39] A. D. Rakic, A. B. Djurisic, J. M. Elazar, and M. L. Majewski, "Optical properties of metallic films for vertical-cavity optoelectronic devices," *Applied Optics,* 37(22), 5271-5283 (1998).